Investigation of interface electronic structure of annealed Ti/Ni multilayers

2005 J. Phys.: Condens. Matter 17 7465

(http://iopscience.iop.org/0953-8984/17/48/002)

INSTITUTE OF PHYSICS PUBLISHING JOURNAL OF PHYSICS: CONDENSED MATTER

J. Phys.: Condens. Matter **17** (2005) 7465–7488 doi:10.1088/0953-8984/17/48/002

Investigation of interface electronic structure of annealed Ti/Ni multilayers

Pramod Bhatt and S M Chaudhari[1]

UGC-DAE Consortium for Scientific Research, University Campus, Khandwa Road, Indore-452017, MP, India

E-mail: smc@csr.ernet.in and pramod@csr.ernet.in

Received 25 April 2005, in final form 25 August 2005
Published 11 November 2005
Online at stacks.iop.org/JPhysCM/17/7465

Abstract

The present paper deals with a systemic investigation of the interface electronic structure of as-deposited as well as annealed Ti/Ni multilayer (ML) samples up to 400 °C using core level and valence band (VB) photoemission techniques. For this purpose [Ti(50 Å)/Ni(50 Å)] × 10 ML samples have been prepared by employing an electron beam evaporation technique under ultrahigh vacuum conditions.

The depth profile core level photoemission investigation carried out on annealed ML samples indicates a gradual change in the nature of the electronic bonding at the interface with temperature. In particular the ML samples annealed at 300 and 400 °C clearly show shifts in the Ni $2p^{3/2}$ and Ti $2p^{3/2}$ core levels towards the higher binding energy side as compared to as-deposited samples, suggesting the formation of a TiNi alloy phase at the interface. The corresponding VB spectra also show appreciable changes and provide strong evidence for TiNi alloy formation. Further confirmation of this alloy phase formation is clearly reflected in the x-ray diffraction measurements carried out on these samples. The recorded x-ray diffraction patterns show a solid state reaction leading to amorphization when the ML sample is annealed at 300 °C and recrystallization to a TiNi alloy phase at the annealing temperature of 400 °C.

In order to determine the charge transfer between Ti and Ni atoms in the formation of the TiNi alloy phase, the $2p^{3/2}$ core levels and the x-ray excited Auger regions of Ti and Ni were carefully investigated. The experimentally measured core level shifts for Ti and Ni were both found to be positive, leading to the conclusion that electronegativity criteria cannot be used to decide the direction of charge transfer in this case. The observed shifts in modified Auger parameters determined from recorded experimental data show a positive value for Ti and a negative one for Ni. This provides clear evidence that the direction of charge transfer is from Ni to Ti atoms during the formation of the TiNi alloy at the

[1] Author to whom any correspondence should be addressed.

interface. The charge on ionized atoms calculated by using a simple electrostatic model indicates similar trends for the charge transfer deduced from Auger parameters and chemical shifts. In addition to this, areas under the core level peaks have been calculated by employing Shirley and Touggard background methods. The difference between the backgrounds, when normalized with respect to the elemental values, provides information about the density of states at the Fermi level (E_F). The density of states at E_F calculated in this way shows reductions in values for both Ti and Ni when the ML sample is annealed at different temperatures. This is in complete agreement with corresponding theoretically calculated densities of states.

1. Introduction

It is now well established that thin film ML structures when synthesized on the nanometre length scale exhibit unusual physical properties and, because of this, they are recognized as potential candidates for various technological applications. Among the vast varieties of thin film ML structures that exist today, Ti/Ni is of special interest for the following two reasons. Firstly, the Ti/Ni MLs are found to be useful for applications in the fields of soft x-rays [1, 2] and neutron optics [3], where they are considered as optical elements such as highly reflecting mirrors, supermirrors, polarizers and monochromators. Further, TiNi alloy prepared in thin film form shows an interesting shape memory effect [4] and this has been utilized to develop different microelectromechanical systems (MEMS) such as cantilevers and actuators. In addition to this, TiNi materials are biocompatible; therefore they are used in making biomedical systems [5–8]. The second reason for which Ti/Ni MLs are identified as interesting is because they show amorphization through solid state reaction (SSR) [9, 10]. The Ti/Ni ML system satisfies the main conditions for SSR. These conditions are a large negative heat of mixing, anomalous fast diffusion of Ni atoms into the Ti layer and a low mobility for one of the elements in the amorphous phase. Because of this, Ti/Ni MLs are considered as model objects for studying the basic phenomena of SSR and phase transformation.

Generally ML structures are susceptible to thermal degradation and show deterioration in their physical properties. In order to achieve optimum performance of a particular ML structure either in device application or when creating a desired physical property, it is essential to understand the role of various microstructural parameters such as the individual layer thickness, surface and interface quality in terms of roughness, width and electron density gradation. The quality of the interface is strongly influenced by interdiffusion, intermixing and phase formation at the interface; it is therefore very interesting to investigate the role of various microstructural parameters at the interface. In this respect, while many structural and thermal stability studies on Ti/Ni MLs have been extensively reported in the literature [11–15], surprisingly few reports are available on corresponding magnetic [16–21] and electronic property [16, 22] investigations. Recently, in our investigation carried out on annealed Ti/Ni MLs [16], we have reported a correlation study of structural, chemical and magnetic properties and it has been found that the Ti/Ni ML structures show amorphization in the temperature range of 300–400 °C. However, to the best of our knowledge no studies have been reported so far in the literature regarding the interface electronic property investigation of as-deposited as well as annealed Ti/Ni ML structures. Since the Ti/Ni ML system undergoes interesting structural transformations upon thermal treatment, it is expected that such a system will also show interesting structure dependent electronic properties. The aim of the present paper is therefore

to investigate the interface electronic properties of as-deposited as well as annealed Ti/Ni ML structures in detail. In particular, the emphasis has been placed on determining carefully the shift in core level binding energy positions of Ti and Ni, the chemical shift, changes in Ni 3d satellites and shifts in modified Auger parameters, to determine the direction of charge transfer when TiNi phase is formed at the interface. Both core level and VB spectroscopy along with the depth profile technique have been used for this purpose, to provide complete information about the shift in core levels, evolution of the VB, change in satellite structure and nature of the charge transfer when samples are alloyed at the interface due to annealing treatment.

2. Experimental details

Ten bilayers of Ti/Ni ML structures each having the layer thickness of 50 Å were deposited on float glass substrates using the electron beam evaporation technique under ultrahigh vacuum (UHV) conditions [23]. In order to avoid contamination during deposition, the system was thoroughly baked to a temperature of 200 °C for 12 h to achieve a background pressure of $\sim 1 \times 10^{-10}$ Torr. The quality of the vacuum was checked using a residual gas analyser (RGA) before the start of deposition. The deposition was carried out at the background pressure of $\sim 5 \times 10^{-10}$ Torr. Deposition of both Ti and Ni layers was carried out at a rate of 0.1 Å s^{-1}. During deposition the thickness of each layer was monitored using a water-cooled quartz crystal thickness monitor. Since Ti is the top deposited layer and has a higher affinity to oxygen, a C capping layer of 20 Å is also deposited on the top in order to avoid oxidation when there is exposure to the atmosphere for other measurements. This C capping layer was deposited in the same run. For this purpose, pure carbon was loaded in another pocket of the e-gun along with Ti and Ni and evaporated on top after ML deposition was completed. ML samples prepared in this way were annealed at 100, 200, 300 and 400 °C for 1 h under a high vacuum of the order of 1×10^{-7} Torr. The structural characterizations of these as-deposited and annealed ML samples were carried out using an x-ray diffraction (XRD) technique. All the XRD measurements were carried out on a diffractometer (Rigaku model No RTP300 RC) equipped with an 18 kW rotating Cu anode as a source of x-rays.

Core level and VB measurements on as-deposited as well as annealed ML samples were carried out using the photoelectron spectroscopy (PES) beamline workstation installed on Indus-1 [24]. This workstation consists of a 180° hemispherical analyser (Omicron EAC-125), a μ-metal experimental chamber, a sample preparation chamber and a twin anode x-ray source. Other facilities, such as *in situ* sample heating up to 600 °C, cooling to LN_2 temperature and an argon ion source for depth profiling, are also incorporated in this workstation. Depth profilings of the ML samples were carried out using an Ar^+ ion etching gun (SPECS model No-IQE 11/35). Knowing that energetic Ar^+ ions used for sputtering may cause intermixing between C, Ti and Ni elements leading to broadening of the interface profile, we have used 2 keV Ar^+ ions (in a flux of $\sim 3 \times 10^{10}$–10^{11} ion cm^{-2}) for etching the samples. In each case, sputtering was also carried out at oblique incidence geometry, so the penetration depth of the Ar^+ ions is reduced further. The above value of the ion energy was decided on the basis of a calculation carried out using the SRIM computer code [25]. All core level spectra presented in this investigation were recorded using Mg Kα radiation at a constant analyser pass energy of 50 eV. The spectrometer was calibrated using the Pt $4f^{7/2}$, Au $4f^{7/2}$ and Ag $3d^{5/2}$ core level lines. Since all the samples were metallic in nature, we have not observed any charging of the samples during measurements. The VB photoemission measurements on as-deposited and annealed ML samples were recorded using the PES beamline installed on the Indus-1 synchrotron radiation source at 134 eV photon energy. The details of this PES beamline are reported elsewhere [26]. The contamination of the sample surface due to oxygen was checked

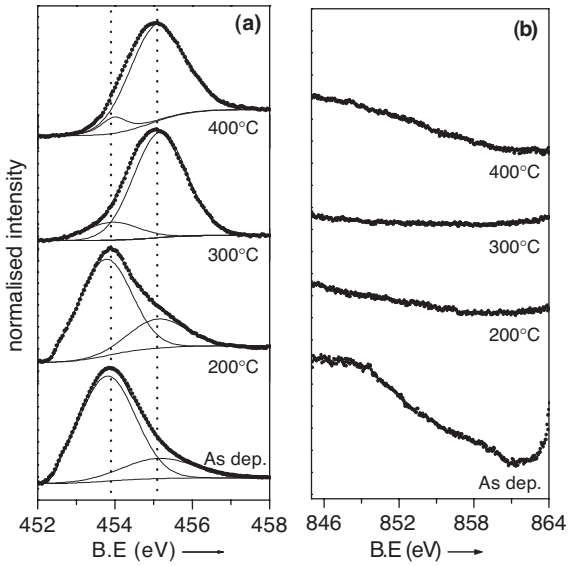

Figure 1. Core level spectra for as-deposited and annealed ML samples corresponding to 0 min of sputtering time; (a) fitted Ti $2p^{3/2}$ and (b) Ni $2p^{3/2}$ core level regions.

by monitoring the oxygen 1 s signal and no appreciable oxygen presence on the sample surface was detected.

3. Results and discussion

3.1. $2p^{3/2}$ *core level analysis*

Figure 1(a) shows measured and fitted x-ray photoelectron (XP) spectral data corresponding to as-deposited ML samples as well as ones annealed at 200, 300 and 400 °C. The spectra recorded for as-deposited ML samples show a peak at the binding energy position of 453.7 eV, matching well with the reported values [27, 28]. The sample annealed at 200 °C shows no shift in the Ti $2p^{3/2}$ peak binding energy position except some reduction in intensity. However, the ML samples annealed at 300 and 400 °C show shifts in the $2p^{3/2}$ peak position to the higher binding energy side. These shifted peaks at 455.0 eV are assigned to the formation of TiC compound. At this higher temperature of annealing the presence of a TiC peak is evident, since a 20 Å C capping layer is purposely deposited on top of the ML samples to avoid the oxidation of the samples when they are exposed to the atmosphere after depositions for other measurements. Such formation of TiC is also reported by Mahesh Vadpathak *et al* [22] in their investigation carried out on Ti/Ni MLs. The corresponding XP spectra recorded in the Ni $2p^{3/2}$ spectral region are shown in figure 1(b). The recorded spectra do not show any presence of a peak corresponding to Ni $2p^{3/2}$ up to the annealing temperature of 400 °C because the recorded information is mostly from the top 50 Å thick deposited layer, consisting of Ti and C. In order to get some quantitative information about the atomic percentage concentration, recorded spectra are fitted using an appropriate fitting procedure [29]. From the fitted spectra, it is seen that for an as-deposited ML sample, 93% atomic Ti is present in elemental form while the remaining 7% contribution is due to the formation of TiC compound. This indicates that during deposition, there is formation of small amount of TiC phase. With increased temperature of annealing, the

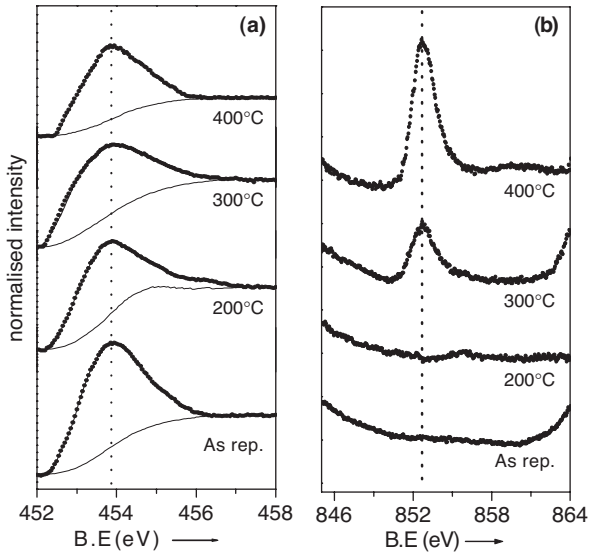

Figure 2. Core level spectra for as-deposited and annealed ML samples corresponding to 15 min of sputtering time; (a) fitted Ti $2p^{3/2}$ and (b) Ni $2p^{3/2}$ core levels.

amount of this phase is found to be increased. In particular, at annealing temperatures of 300 and 400 °C mostly 91% and 96% contributions, respectively, are shown due to the formation of TiC phase.

The fitted Ti $2p^{3/2}$ XP spectra recorded after 15 min of sputtering time for as-deposited and ML samples annealed at 200, 300 and 400 °C are shown in figure 2(a). For depth profiling the ML samples, we have used a sputtering rate of 2 Å min^{-1} for both Ti and Ni layers. This rate was established separately by carrying out experiments on Ti and Ni single-layer films of known thicknesses using the sputtering parameters mentioned in the experimental section. The spectrum corresponding to the as-deposited ML sample shows a peak at the binding energy position of 453.7 eV and this is assigned to elemental Ti. Recorded Ti $2p^{3/2}$ XP spectra for ML samples annealed at 200, 300 and 400 °C show no shift in binding energy position except a decrease in intensity with increasing temperature. This indicates that after 15 min of sputtering, the recorded information is mainly from the top deposited Ti layer. From the fitted spectrum, it is seen that in the case of the as-deposited ML sample after 15 min of sputtering time, 96% Ti is present. At higher temperatures of annealing, the Ti concentration shows a reduction from 96% to 70% at 400 °C, indicating intermixing of the Ti and Ni layers, particularly at higher temperatures of annealing of 300 and 400 °C. The corresponding Ni $2p^{3/2}$ XP spectra are shown in figure 2(b). No Ni $2p^{3/2}$ peak is observed for as-deposited ML samples annealed up to 200 °C. However, ML samples annealed at 300 and 400 °C show the clear presence of an Ni $2p^{3/2}$ peak at the binding energy position of 852.5 eV. This observation also indicates the intermixing at higher temperatures of annealing due to the faster diffusion of Ni atoms into Ti layers. The fitted spectra show around 17% and 30% atomic concentrations of Ni respectively for the ML samples annealed at 300 and 400 °C.

Although Ni is not observed in the case of the ML sample annealed at 200 °C, the corresponding Ti Auger transitions, which are very sensitive to local environmental changes of the atoms, fall in the spectral region of the Ni $2p^{1/2}$ core level and give a clear indication of the changes that have occurred due to annealing at this temperature. The XP Auger spectra

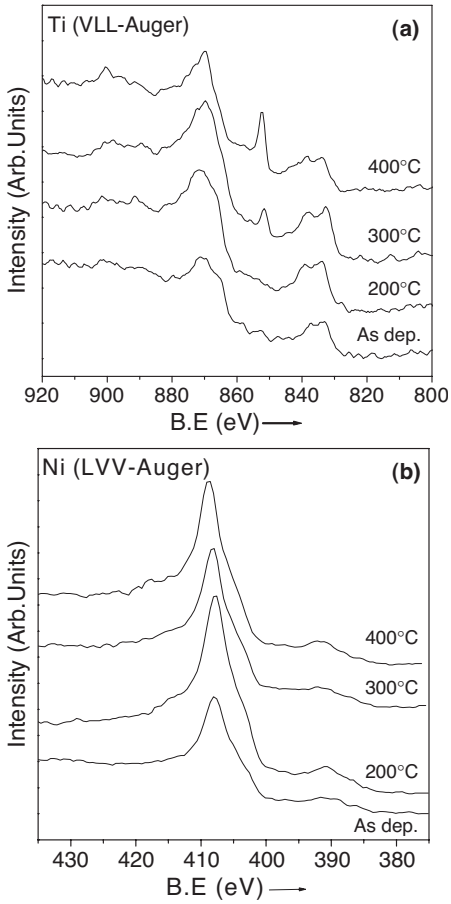

Figure 3. Auger spectra of as-deposited as well as ML samples annealed at different temperatures for (a) the Ti Auger region, recorded after 15 min of sputtering, and (b) the Ni Auger region, after 45 min of sputtering time.

corresponding to as-deposited as well as annealed ML samples at 200, 300 and 400 °C and recorded after 15 min of sputtering time for Ti and after 45 min for Ni are shown in figures 3(a) and (b) respectively. These two figures together provide important information about the changes in the Auger parameters and hence the modifications at the interface with annealing treatment. The peaks at binding energy positions of 865.4 and 871.3 eV (in figure 3(a)) in the case of as-deposited samples are due to the Ti $L_3M_{23}M_{23}$ Auger transition and match well with the reported literature [27, 30]. The sample annealed at 200 °C shows modification in this observed Auger transition. In this case, the Auger peak intensity is observed to be reduced with the shift in binding energy positions to the higher energy side. The well defined Auger peak features in the as-deposited case are merged into one peak structure as the samples are annealed. The further annealing of ML samples at 300 and 400 °C results in a narrowing of the main Auger peak structure. In addition to this, an additional peak at the binding energy position of 852.4 eV is also observed due to the Ni 2p core level. All these changes in the Auger transition as compared to the as-deposited case indicate a substantial modification of the chemical environment due to Ni diffusion at the 200 °C temperature of annealing, while the changes observed at 300 and 400 °C may be due to TiNi phase formation.

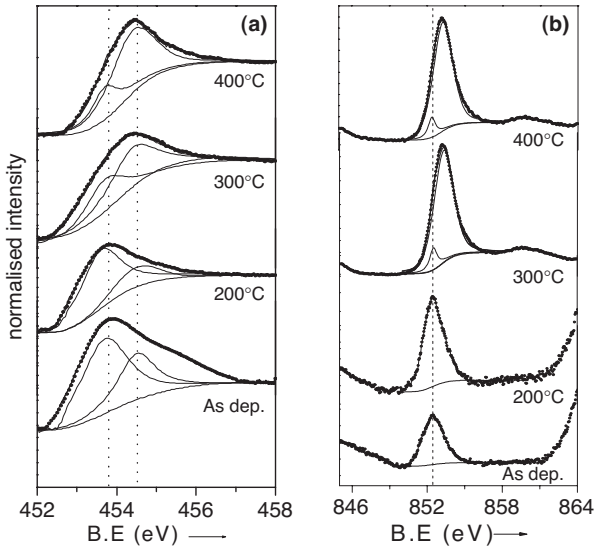

Figure 4. Core level spectra for as-deposited and annealed ML samples corresponding to 30 min of sputtering time; (a) fitted Ti $2p^{3/2}$ and (b) fitted Ni $2p^{3/2}$ core levels.

The fitted Ti $2p^{3/2}$ XP core level spectra recorded after 30 min of sputtering time corresponding to as-deposited and annealed samples are shown in figure 4(a). Considering the sputtering rate of 2 Å min^{-1}, it is expected that the recorded spectra will provide information essentially from the first interface region of the ML samples. The recorded spectrum of the as-deposited sample shows substantial reduction in the Ti $2p^{3/2}$ peak intensity. The corresponding spectrum recorded in the binding energy region of 845–864 eV shows clearly the presence of the Ni $2p^{3/2}$ peak at 852.5 eV (figure 4(b)) suggesting that the information obtained is indeed from an interface region. This indicates intermixing at the interface during deposition. ML samples annealed at 200 °C show further reduction of the Ti $2p^{3/2}$ peak intensity with corresponding increase of the Ni $2p^{3/2}$ peak intensity. After annealing the ML sample at 300 °C, the recorded Ti $2p^{3/2}$ core level spectra show a shift in the Ti $2p^{3/2}$ binding energy position of 0.7 eV from it original position. Similarly the Ni $2p^{3/2}$ peak (figure 4(b)) also shows a shift in binding energy position towards the higher side of 0.6 eV, indicating formation of TiNi phase at the interface. The observed shift in Ti $2p^{3/2}$ and Ni $2p^{3/2}$ in the present case matches well with the values reported by Hillerbrecht *et al* [31] and Shabalovskaya *et al* [32] in the case of TiNi alloy phase formation. Further annealing of the ML sample at 400 °C shows substantial reduction in the Ti $2p^{3/2}$ peak intensity with a shift in the binding energy position of 0.7 eV. The corresponding Ni $2p^{3/2}$ peak also shows a similar shift of 0.6 eV in the binding energy. The calculated atomic percentage Ti concentration is about 11%, which is much less than the observed value of 82% in the case of samples sputtered for 15 min. The fitted spectra show a systematic decrease in Ti atomic concentration with a corresponding increase in the contribution of the TiNi phase at higher temperatures of annealing. Similar trends are also observed in the cases of Ni and TiNi phase concentrations with increase in the annealing temperature.

The fitted Ti and Ni $2p^{3/2}$ core level spectra of as-deposited as well as annealed ML samples recorded after 45 min of sputtering time are shown in figures 5(a) and (b) respectively. In this case the information obtained is mainly from the Ni layers after the first interface. The peak intensity is observed to be drastically reduced with increase in the annealing temperature. At

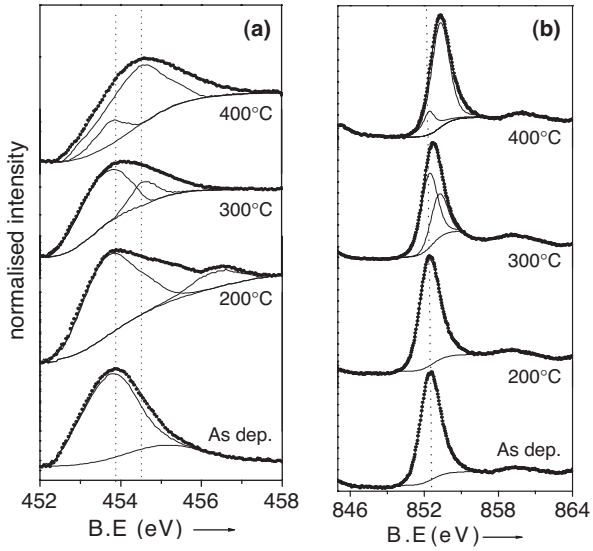

Figure 5. Core level spectra for as-deposited and annealed ML samples corresponding to 45 min of sputtering time at up to 400 °C for (a) fitted Ti $2p^{3/2}$ and (b) fitted Ni $2p^{3/2}$ core levels.

Table 1. Calculated atomic percentage concentration values for as-deposited and ML samples annealed at 200, 300 and 400°C for 0, 15, 30 and 45 min of sputtering time.

	Atomic percentage (%) concentration of as-deposited and annealed samples at												
	0 min			15 min		30 min				45 min			
Samples	TiC	Ti	Ni	Ti	Ni	Ti	TiNi	Ni	TiNi	Ti	TiNi	Ni	TiNi
As deposited	7	93	—	96	—	24	—	76	—	13	—	87	—
200 °C	10	90	—	90	—	20	—	80	—	12	—	88	—
300 °C	91	9	—	82	17	11	40	5	44	10	8	60	22
400 °C	96	4	—	70	30	10	43	6	41	5	45	4	46

400 °C temperature of annealing, mostly the peak corresponding to the TiNi phase is observed. Similar behaviour is also observed in the case of core level spectra recorded for Ni $2p^{3/2}$. These spectra show a reduction in the Ti atomic concentration with a corresponding increase in the Ni concentration in the case of as-deposited and 200 °C annealed ML samples. The ML samples annealed at 300 and 400 °C show reductions in both Ti and Ni. In each case, as mentioned earlier, atomic percentage concentration values are obtained after subtracting the background by using the Shirley method. For fitting the curve, we have used the XPSPEAK-41 computer program [29], which has the option of using mixed Gaussian/Lorentzian functions. The values thus obtained are listed in table 1.

3.2. Background correction and estimation of the DOS at E_F

The background correction techniques can be used effectively to obtain meaningful quantitative information about the changes in the DOS at E_F, particularly when two elements are brought together to form an alloy phase. However, one has to select the appropriate background correction procedure for this. During the formation of the alloy phase, the number and

distribution of the final density of states (DOS) of photoexcited ions show changes. This gives rise to an asymmetry in the shape of the peaks in the spectrum. Such features are referred to as intrinsic loss structures. The intrinsic loss features are therefore indicative of the available states at E_F. Generally the background under the measured spectrum includes both intrinsic and extrinsic loss contributions. The intrinsic contribution can be considered to be associated with the processes within the photoexcited atom and arising from interaction with its nearest neighbours. The extrinsic loss, on the other hand, can be considered as that originating from the transport of electrons to the surface through the solid. Although such losses are inherently mixed and their separation is difficult, they can be approximated using several background correction techniques [33–36]. Among these, the most widely used are the Shirley method [33] and the Tougaard method [37]. In the following paragraph, initially a brief description of these two methods is given and an attempt has been made to extract information about the DOS at E_F from them.

The background corrected spectrum for the Shirley method is given by [33, 38]

$$F_n(i) = J(i) - k_n \sum F_{n-1}(j)\Delta E \tag{1}$$

where $J(i)$ is the intensity in channel i and ΔE is the channel width. The factor k_n is found from the requirement that $F_n(i_{\min}) = 0$. The series converges rapidly and after three to four iterations we have $F_n \sim F_{n-1}$.

The background corrected spectrum for the Tougaard method is given by [37]

$$F_T(E) = J(E) - B_1 \int \{(E' - E)/[C + (E' - E)^2]^2\} J(E')\,\mathrm{d}E'$$

where $C = 1643$ eV^2 and B_1 is an adjustable parameter. For a channel of width ΔE, the background corrected spectral intensity in channel i is obtained from the equation

$$F_T(i) = J(i) - B_1\{[(j - i)\Delta E]/[C + (j - i)^2\Delta E^2]^2\} J(j)\Delta E$$

where $J(i)$ is the intensity in channel i. The maximum kinetic energy $E_{\max}$ is chosen to lie a few electronvolts on the high energy side of the peak structure. The parameter B_1 is adjusted to give $F_T \sim 0$ over a wide energy range below the peak structure. F_T should vanish, not only at a single energy but over a wide energy range. Using a higher value for B_1 will cause $F_T(E)$ to be negative further away from the peak, whereas a lower value for B_1 will result in a failure to get F_T to be zero at any energy. The parameter B_1 can be expressed [37] as

$$B_1 = B \times L/(L + \lambda \cos\theta) \tag{2}$$

where $B = 2866$ eV^2, λ is the inelastic mean free path, θ is the photoelectron emission angle with respect to the surface normal and L is the thickness of the sample. The Tougaard model [39, 40] gives a very good approximation of the extrinsic losses from *a priori* principles. The removal of the extrinsic background would therefore leave a peak with a strong intrinsic tail. The Tougaard model is well suited for transition metal use. The total background is the one that requires no *a priori* knowledge of the peak shape and spectrum structure. This type of background is best modelled by the Shirley method. This simply assumes that the total background at any energy is proportional to the integrated intensity at higher energy with the condition that the background matches the spectrum outside the region of the peak within a small energy range. The difference between these two backgrounds should therefore correspond to the intrinsic loss feature and hence to the distribution of the final states. The Ti $2p^{3/2}$ and Ni $2p^{3/2}$ core level spectra are therefore fitted by both Shirley and Tougaard methods and are shown in figures 6(a) and (b) respectively. Similarly, the areas under the Ti $2p^{3/2}$ and Ni $2p^{3/2}$ peaks have also been estimated in the case of as-deposited as well as ML samples annealed at 200, 300 and 400 °C. The values corresponding to 15, 30 and 45 min of

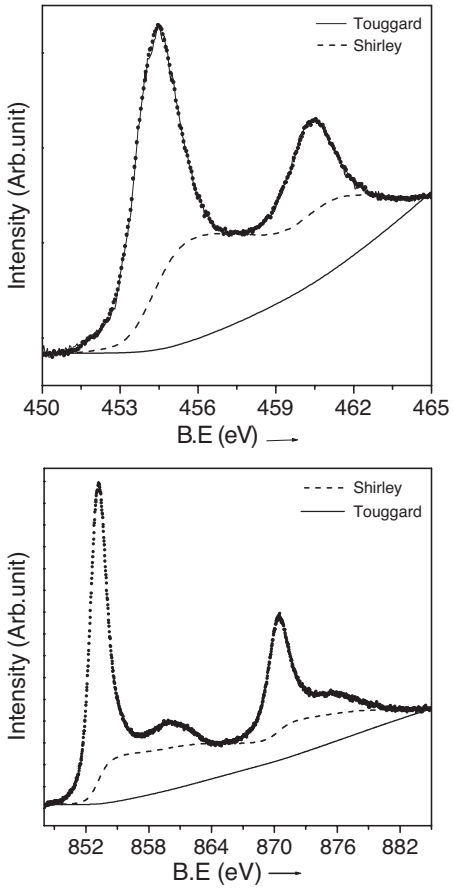

Figure 6. Fitted core level spectra of (a) Ti 2p and (b) Ni 2p with Shirley and Tougaard backgrounds.

sputtering time intervals in each case are listed in table 2. The intrinsic loss features obtained as differences between two backgrounds are normalized with respect to the corresponding elemental values of Ti and Ni. For normalization, data presented in figures 6(a) and (b) have been used. The normalized data represent the DOS at E_F. It can be seen that, as compared to the elemental data for Ti and Ni, the DOS at E_F are found to be decreased with increasing annealing temperature, both for Ti and for Ni. The successive decrease in the DOS of Ti in the cases of samples annealed at 200, 300 and 400 °C and sputtered for 15 min is due to diffusion of Ni atoms into Ti layers. This result is consistent with the conclusion drawn from the corresponding recorded Ti 2p core level spectra, where we observed a decrease in atomic percentage concentration of Ti with increase in the annealing temperature. For 30 min of sputtering and annealing at different temperatures, the Ti DOS are further reduced; however, the Ni DOS show increases in value, particularly at 300 and 400 °C annealing temperatures. As discussed earlier in section 1, the clear shift in binding energy of the recorded core level spectra of Ni $2p^{3/2}$ indicates the formation of TiNi phase at the interface region and hence the observed enhancement in the DOS in this case can be attributed to TiNi phase formation. Similar behaviour is also observed for samples annealed at 400 °C and sputtered for 45 min. Thus the normalized background difference method can provide useful information about the

Table 2. Area under the $2p^{3/2}$ core levels of Ti and Ni fitted with both Shirley and Tougaard background models for as-deposited and 200, 300 and 400 °C annealed ML samples with different sputtering time intervals.

		As dep.		200 °C		300 °C		400 °C	
Samples		Ti $2p^{3/2}$	Ni $2p^{3/2}$	Ti $2p^{3/2}$	Ni $2p^{3/2}$	Ti $2p^{3/2}$	Ni $2p^{3/2}$	Ti $2p^{3/2}$	Ni $2p^{3/2}$
15 min	Shirley	12 215.0	—	10 069.2	—	7 250.0	1 046.6	7 053.1	9 473.4
	Tougaard	29 434.6	—	24 977.5	—	20 238.0	2 150.2	14 825.2	15 604.9
Difference		17 219.6	—	14 908.3	—	13 110.0	1 104.0	7 773.3	6 131.5
Normalized		1.0	—	0.86	—	0.76	0.01	0.45	0.08
30 min	Shirley	14 321.7	2 624.5	10 135.1	8 932.0	9 298.5	72 090.7	5 836.5	75 942.6
	Tougaard	27 256.9	3 562.6	19 596.8	12 414.2	18 307	99 499.8	14 465.9	111 393.2
Difference		12 935.2	938.6	9 461.6	3 482.2	9 008.5	27 409.1	8 629.4	35 450.6
Normalized		0.75	0.01	0.54	0.04	0.52	0.37	0.50	0.48
45 min	Shirley	4 915.71	88 946.6	9 476.9	64 164.2	4 364.0	55 929.1	4 461.7	52 396.3
	Tougaard	6 687.9	162 252.0	11 177.2	126 820.2	5 324.1	112 854.6	6 434.3	95 806.8
Difference		1 772.4	73 306.0	1700.2	62 656.0	960.1	56 925.5	1 473.3	43 410.5
Normalized		0.1	1.0	0.09	0.85	0.05	0.77	0.08	0.59

chemical change that has occurred due to the thermal treatment in the constituent elements of Ti/Ni MLs. Similar work has also been carried out recently by Seablot *et al* [41] on amorphous TiNi alloy thin films with different Ni atomic compositions.

3.3. Nature of the charge transfer in Ti/Ni annealed multilayers

From the discussion on Ti $2p^{3/2}$ and Ni $2p^{3/2}$ core level spectra and the corresponding atomic percentage concentration values listed in table 1 for ML samples annealed at different temperatures, it is seen that Ti and Ni show mostly metallic character in the cases of samples annealed up to 200 °C and sputtered for 15 min. In addition to this, the recorded Ti $2p^{3/2}$ and Ni $2p^{3/2}$ core levels for 30 min of sputtering time show a slight intermixing of layers at the interface during deposition. The extent of this mixing is found to be increased when the sample is annealed at 200 °C. The higher temperature annealing at 300 and 400 °C, results in a clear shift in binding energy position, confirming the formation of TiNi alloy phase. The experimentally observed core level shifts in binding energy position of Ti $2p^{3/2}$ and Ni $2p^{3/2}$ are listed in table 3. When compared with the respective elemental values, substantial differences in binding energy positions are seen to exist for TiNi phase formation. This indicates a significant change in the electronic configuration of Ti and Ni when they are alloyed. The reported value of the electronegativity for Ti is 1.5 while for Ni it is 1.9 [42]. On the basis of the electronegativity criteria, the $2p^{3/2}$ core level of Ti should show a positive shift while Ni $2p^{3/2}$ should show a negative shift if the charge transfer occurs from Ti to Ni. However, the data in table 3 show positive shifts for both Ti and Ni $2p^{3/2}$ core levels, indicating that the electronegativity criteria cannot be applied to the experimentally observed core level shift to obtain a conclusion about the direction of the charge transfer between the constituent elements. Therefore, in order to obtain information on the charge transfer between titanium and nickel, we have investigated the Ti and Ni Auger regions of the spectra. The normalized spectra in the x-ray excited Auger regions of titanium ($L_{2,3}M_{2,3}M_{2,3}$) and nickel (L_3VV) are shown in figures 3(a) and (b) respectively. The binding energies of the most prominent peaks in these regions are also listed in table 3.

Table 3. Calculated core level shift, Auger parameter and shift in Auger parameter for as-deposited and annealed ML samples.

	Core level B.E. (eV)		Core level shift ΔE (eV)		B.E. (eV) of intense Auger peak		Auger parameter α'		Shift in Auger parameter $\Delta\alpha'$	
Sample	Ti-$2p^{3/2}$	Ni-$2p^{3/2}$	Ti	Ni	Ti	Ni	Ti	Ni	Ti	Ni
As-deposited	453.7	852.5	—	—	871.3	407.6	835.0	1698.1	—	—
200 °C	453.6	852.5	—	—	871.3	407.6	835.0	1698.1	—	—
300 °C	454.4	853.1	+0.7	+0.6	870.3	408.4	836.6	1697.7	1.6	−0.4
400 °C	454.4	853.1	+0.7	+0.6	870.1	408.7	836.8	1697.5	1.8	−0.6

3.3.1. Auger parameters. The Auger parameter (AP) has been found to be very sensitive to changes in the chemical state of the constituents [43]. The modified AP (α') is defined by the equation

$$\alpha' = h\nu - \mathrm{BE}_{\mathrm{Auger}} + \mathrm{BE}_{\mathrm{PE}} \tag{3}$$

where $h\nu$ is the energy of the incident photons, $\mathrm{BE}_{\mathrm{Auger}}$ is the binding energy (BE) of the prominent peak in the Auger region and $\mathrm{BE}_{\mathrm{PE}}$ is the BE of the photoelectric peak. The advantage of this modified AP is that it becomes independent of the x-ray source used for excitation and facilitates comparison with values obtained from different instruments. The AP (α') and shift in AP ($\Delta\alpha'$) values obtained in the present study are listed in table 2.

A change in the AP is a measure of a change in the extra-atomic relaxation, or screening of the final state ion in the Auger transition by electrons from neighbouring atoms or by conduction electrons [44–46]. The chemical shift in the AP is to a first approximation half of the difference in this relaxation energy, or twice the difference in the relaxation energy associated with the singly charged final ion states in the photoelectric transition. Snyder [47] used Slater's rules for the atomic shielding constant and the Slater–Zener expression for the energy of an atom and has shown that the relaxation energy for the core hole state is proportional to the number of electrons in shells outside the core hole. In addition to this, the relaxation energy is found to be independent of the nuclear charge and quadratic in the charge of the shielding constant for each shell upon core hole formation. Adopting Snyder's theoretical approach for the present case, the positive values of $\Delta\alpha'$ for Ti and negative values for Ni show that there is a charge transfer from nickel to titanium during formation of the TiNi alloy phase. As can be seen from the listed $\Delta\alpha'$ values in table 2, no shift in Auger parameters has been observed corresponding to ML samples annealed up to 200 °C. The ML samples annealed at 300 and 400 °C show a positive shift for Ti and a negative shift for Ni. This shows that there is charge transfer from Ni to Ti during TiNi phase formation at the interface at these temperatures of annealing. The calculated atomic percentage values listed in table 1 show that the TiNi alloy phase formed at the interface has about 50–50 composition.

3.3.2. Chemical shift. The core level shift is a very significant parameter in XP spectroscopy (XPS). It provides the most direct information about the change of the character of the bonding due to alloying and charge transfer between the atoms [48, 49]. If we denote by $\Delta\varepsilon(i)$ the change of the Hartree–Fock one-electron energy of the core level i due to the redistribution of the valence electrons upon alloying, we can write [49] the core level shift $\Delta E(i)$ as

$$\Delta E(i) = -\Delta\varepsilon(i) + \Delta\varepsilon_{\mathrm{F}} - \Delta E_{\mathrm{r}}. \tag{4}$$

We see that experimentally measured core level shift $\Delta E(i)$ is not simply determined by $\Delta\varepsilon(i)$ alone; there are also contributions from two more terms. The term $\Delta\varepsilon_F$ arises because $\Delta\varepsilon(i)$ is relative to the vacuum level, whereas E_B is measured experimentally with respect to the Fermi level of the sample. The second term ΔE_r is the difference of relaxation energies in the presence of core holes between the alloy and the metal. This final state effect in XPS has been neglected or treated incompletely in most of the previously reported works on core level shifts. However, studies [50, 51] on metallic systems clearly show the importance of this final state screening energy. A theoretical calculation [52] predicts that ΔE_r is generally important and can be as large as 1–2 eV in some binary alloys, so the inclusion of this term can change the conclusion about the direction and magnitude of the charge transfer in alloy systems. In the literature [53–57] the Mössbauer shift and core ionization energy shift have been used to provide some insight into the degree of charge transfer in binary alloys. An earlier potential model has been used to analyse these core level shifts, but this was plagued by a host of difficulties. The main problem is that one cannot analyse ionization energy shifts to give the ground state charge distribution without making a correction for the final state charge rearrangement (screening of the core hole, or relaxation). In recent work carried out on Ag–Pd and Pd–Mn alloy systems, Olovsson *et al* and Abrikosov *et al* [58, 59] have reported the precisely calculated core level and Augur energy shifts obtained from a 'complete screening picture' using first-principles theory. In this 'complete screening picture' the conduction electrons have attained a fully relaxed configuration in the presence of the core hole. Therefore in this model, both the initial and final state effects are fully included and are treated within the same scheme and not as two separate contributions. However, a rigorous theoretical treatment with elaborate computational work is required in order to take into consideration the effect of these terms. An alternative simple approach for determining the relaxation energy term is to obtain this value from experimentally measured Auger parameter shifts. They depend on the change in the potential at the core when an inner shell electron is removed. The detailed treatment of this method has been reported by Thomas *et al* [60].

Thus, from above discussion, it is clear that the experimentally observed core level shifts (ΔE) may be due to the different local chemical and electronic environments of the central atom and can be expressed in terms of the various components by

$$\Delta E = \Delta E_c + \Delta E_{ch} + \Delta E_R. \tag{5}$$

where ΔE_c is the contribution due to the configuration changes (distribution of electrons among s, p and d states, as appropriate), ΔE_{ch} is the chemical shift due to the charge transfer and ΔE_R is the relaxation shift. Ignoring ΔE_c, we have calculated the chemical shifts for Ti $2p^{3/2}$ and Ni $2p^{3/2}$ core levels using this relation. The changes in AP, $\Delta\alpha'$, have been used for calculating ΔE_R. The values of the chemical shifts thus obtained for the samples studied are listed in table 4. We observe a negative chemical shift for the titanium $2p^{3/2}$ core level and a positive chemical shift for the nickel $2p^{3/2}$ core level in the ML samples annealed at 300 and 400 °C. The chemical shift data indicate the direction of charge transfer from nickel to titanium for ML samples annealed at 300 and 400 °C.

The chemical shifts ΔE_{ch} to a good approximation reflect the changes in charge, Δq, on the ionized atom, i.e. $\Delta E_{ch} \propto \Delta q$. A simple model can be applied to deduce a relationship between the chemical shifts and Δq. The chemical shift can be considered to be a change in the electrostatic potential felt by the core electrons when a certain amount of charge is removed from the spherical shell of one atom and transferred to the spherical shell of the neighbouring atom. According to this model,

$$\Delta q = f \times \Delta E_{ch} \tag{6}$$

Table 4. Interatomic distances, calculated chemical shifts and charge transfers in as-deposited and annealed ML samples at different temperatures.

		Interatomic distance (f)		Chemical shift (ΔE_{ch})		Charge transfer (Δq)	
Samples	R_A (Å)	Ti	Ni	Ti	Ni	Ti	Ni
As-deposited	—	—	—	—	—	—	—
200 °C	—	—	—	—	—	—	—
300 °C	2.40	−0.26	−0.17	−0.9	+1.0	+0.234	−0.170
400 °C	2.40	−0.26	−0.17	−1.1	+1.2	+0.286	−0.204

where $f = [14.4(1/R_A - 1/R_M)]^{-1}$. The factor 14.4 accounts for the numerical constants necessary to have the energy in eV when the radius is expressed in Å and the valence charge in units of the electron charge. Here R_A is the interatomic distance and R_M is the atomic radius of the metal. The values of R_A and R_M have been obtained from previously reported EXAFS studies [61] and from [62] and are listed in table 4. The values of Δq in the case of ML samples annealed at 300 and 400 °C have been calculated using the above equation and are listed in table 4. We observe negative values for Ni and positive values for Ti with reference to the corresponding elements. These values indicate that the direction of charge transfer is from Ni to Ti in these alloy films. This is in complete agreement with the direction of charge transfer deduced from the AP and the chemical shift data.

3.4. XRD measurements

In order to support the results discussed in earlier sections concerning the formation of TiNi alloy phase due to annealing treatment, we have carried out XRD measurements on ML samples annealed up to 400 °C. The recorded XRD patterns are shown in figure 7. The XRD pattern for as-deposited samples show mainly crystalline peaks due to Ti(002) and Ni(111) at 2θ values of 38.4° and 44.4° respectively [63]. There is no appreciable change in the recorded XRD pattern for the ML sample annealed at 200 °C. However, an interesting structural change is observed at 300 °C annealing temperature. The recorded pattern shows a clear broad hump around a 2θ value of 44.1° indicating amorphization of the as-deposited ML structure. The amorphization at this temperature is triggered by diffusion of one element. In the case of the Ti/Ni ML structure, Ni atoms are more mobile [64] and would start diffusing into the relatively immobile lattice of Ti layers. The faster diffusion of Ni atoms at these lower temperatures is the main cause of SSR leading to amorphization at the interface in this ML structure. The ML sample annealed at 400 °C again shows crystalline peaks at 2θ values of 37.7° and 44.1° due to recrystallization of ML samples and also shows shifts in the Ti(002) and Ni(111) peak positions. These new peaks are assigned to the TiNi alloy phase [63]. Thus the XRD spectrum clearly indicates the recrystallization and formation of TiNi phase at 400 °C annealing temperature.

3.5. Valence band photoemission measurements

In this section, we present VB photoemission measurements carried out on as-deposited and annealed Ti/Ni ML samples in order to follow the evolution and modifications due to the annealing treatment. The VB XP spectra are recorded each time after sputtering the sample for 15, 30 and 45 min using Mg Kα radiation ($h\nu = 1253.6$ eV), while a synchrotron radiation source is used to record the VB spectra at lower photon energies of 134 eV and below. Figure 8 shows VB XP spectra for as-deposited and annealed ML samples sputtered for different time

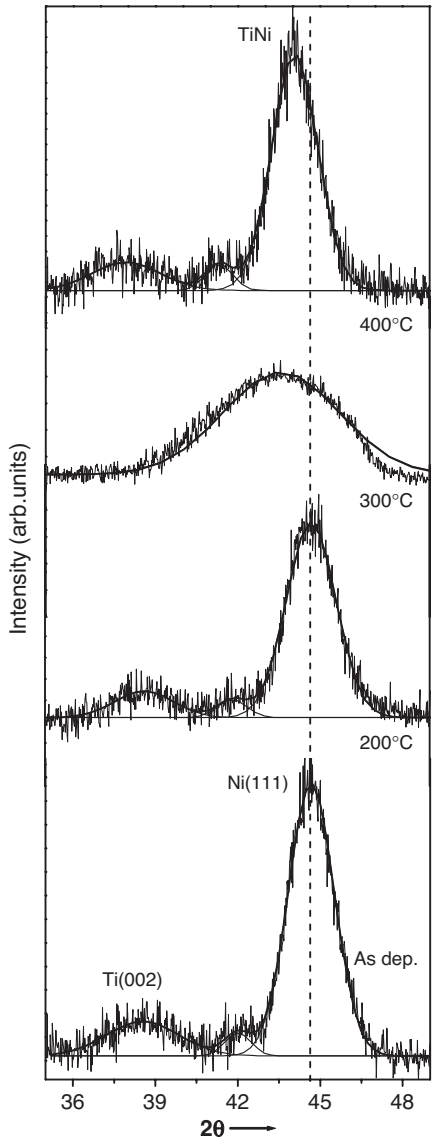

Figure 7. XRD patterns of as-deposited and ML samples annealed at 200, 300 and 400 °C.

intervals of 15, 30 and 45 min. The spectra corresponding to 0 min of sputtering time for each case are not shown in this figure, since carbon is deposited as the top layer and the recorded spectrum resembles that of the amorphous carbon VB. The VB spectra recorded for the as-deposited ML sample sputtered for 15 min show mixed features due to the photoemission from Ti 3d and TiC bands. However, the spectra recorded after 30 min of sputtering time show a clear emission at 0.8 eV due to the Ni 3d band. It is to be noted that, considering the 2 Å min^{-1} sputtering rate, the recorded spectrum in this case is mostly obtained from the first interface region of the ML structure. A spectrum recorded after 45 min of sputtering time shows photoemission due to the Ni 3d band at the binding energy position of 0.8 eV. The centroid of this band is located at 1.35 eV from E_{F}. In addition to this, a peak at 6.1 eV is

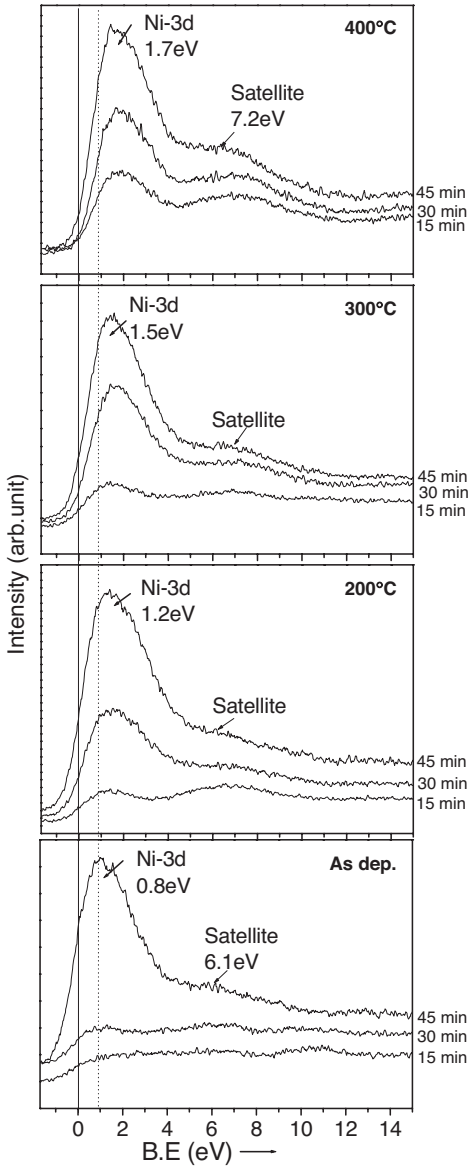

Figure 8. VB XP spectra of as-deposited and ML samples annealed at 200, 300 and 400 °C and sputtered for 15, 30 and 45 min.

also seen and this is assigned to the Ni 3d satellite, indicting that the observed VB features are due to the elemental Ni and match well with the VB spectra reported in the literature [65, 32]. No photoemission VB feature corresponding to Ti 3d states is observed. It is known that the photoionization cross-section of the Ti 3d state is one to two orders of magnitude smaller than that of Ni [66] at this photon energy of excitation. The recorded VB XP spectrum therefore mainly reproduces the shape of the local density of Ni 3d states.

The VB spectra recorded for the as-deposited ML sample using the synchrotron radiation source at 134 eV are shown in (figure 9(a)). The recorded spectra after 15 min of sputtering

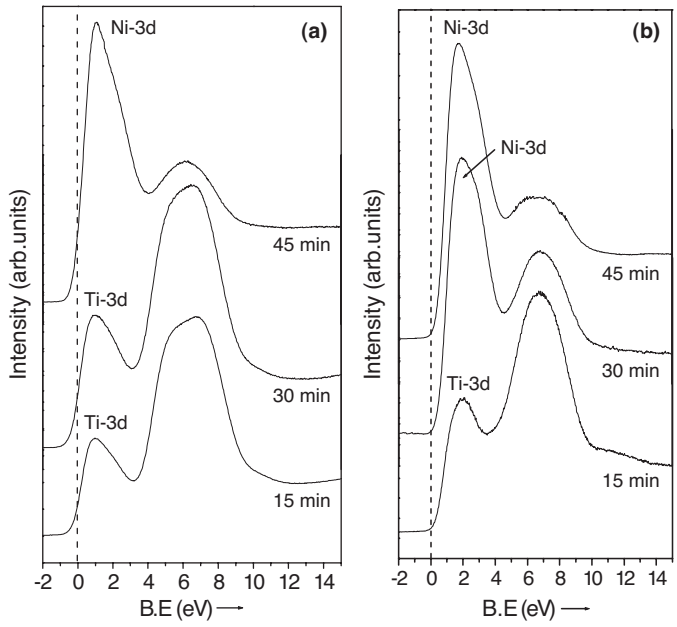

Figure 9. VB spectra of (a) as-deposited and (b) 400 °C annealed ML samples recorded using 134 eV synchrotron radiation after 15, 30 and 45 min of sputtering.

time clearly show a photoemission peak corresponding to Ti 3d at 1.0 eV. Further, a strong emission at binding energy position at 6.8 eV is also observed due to O 2p and resembles the Ti_2O_3 VB spectrum reported in the literature [67]. This is expected because, in deposited Ti/Ni ML structures, Ti is the top deposited layer and it may have oxidized during exposure to air, even though a 20 Å protective C capping layer was deposited to prevent oxidation. The spectra recorded after 30 min of sputtering time show overall features similar to those for the 15 min of sputtering sample. No photoemission peak due to the Ni 3d band is observed in spite of the fact that the spectrum obtained is mostly from the interface region. In this situation, one would expect a contribution due to the Ni 3d density of states near the Fermi level. This is because of the large difference in the d photoionization cross-section between Ti and Ni metals and suggests more favourable conditions at lower photon excitation energy for the study of Ti bands, which does not develop in recorded VB XP spectra. However, the spectrum corresponding to 45 min sputtering time shows feature like those for elemental Ni, because the signal obtained is mostly from the Ni layer after crossing the interface region. Thus depth profile VB photoemission measurements carried out at the photon energy of 1256.6 eV using the Mg Kα excitation source are mainly dominated by photoemission due to Ni 3d states, while the spectra recorded using synchrotron radiation at 134 eV show the presence of an emission band mostly due to Ti 3d states. These measurements together indicate the intermixing of Ti and Ni layers during deposition at the interface without any chemical bonding between them.

The VB XP spectra recorded for the ML sample annealed at 200 °C are shown in figure 8. The spectrum recorded after 15 min of sputtering of the sample shows broad features around 0.9 and 6.1 eV. The observed emission bands at these binding energy positions are assigned to Ni 3d and its satellite respectively. The observation of Ni 3d and its satellite is a consequence of diffusion of Ni atoms due to faster mobility into the Ti layer at this temperature of annealing,

as mentioned earlier in the text. The enhancements in the intensity of these emission bands are more clearly seen as the temperature of annealing is increased to 300 and 400 °C, indicating the still faster diffusion of Ni atoms. The VB spectra recorded after 30 min of sputtering time show an emission band due to Ni 3d and its satellite at binding energy positions of 1.2 and 6.4 eV, which are observed to be shifted from its corresponding elemental Ni 3d band position. The recorded VB spectra clearly show emission at 1.5 and 1.7 eV due to Ni 3d bands at 300 and 400 °C temperatures of annealing respectively. The observed shift in the Ni 3d binding energy position to the higher energy side as compared to its elemental value may arise due to the microalloy formation of TiNi phase at the interface and the subsequent increase in the extent of this phase at 300 °C and 400 °C temperatures of annealing. The VB spectra of the ML sample recorded after 45 min of sputtering time also clearly show a shift in the Ni 3d band as well as its satellite peak position when the ML sample is annealed at 400 °C. The observed shift is 0.9 eV from the value for the as-deposited case for the Ni 3d band, while it is 1.1 eV for the Ni 3d satellite. This observed shift and the reduced density of states at the Fermi level are consequences of the formation of TiNi alloy phase at the interface due to the annealing treatment. A similar shift in the Ni 3d photoemission band and reduction in the density of states due to the formation of TiNi alloy phase are also reported by Shabalovskaya *et al* [32] and Fuggle *et al* [68] in their investigation on bulk Ti and Ni based alloy and intermetallic compounds.

The VB spectra recorded at 134 eV using synchrotron radiation for the ML sample annealed at 400 °C (figure 9(b)) and etched for 45 min show behaviour similar to that discussed above. In this case, the position of the Ni 3d photoemission band is observed to be shifted by 0.9 eV as compared to as-deposited position. The Ni 3d satellite observed at 7.2 eV is also shifted by 1.1 eV. Recorded VB spectra obtained after 30 and 15 min of sputtering time mainly show mixed photoemission features due to Ni and Ti bands. In particular, the peak close to the Fermi level is due to the Ti 3d band, which is not observed in the VB XP spectra recorded. The presence of a Ti DOS near the Fermi level is clearly seen when the spectra are recorded at photon energy even lower than 134 eV (figure 10(b)). In addition to this, spectra recorded at lower photon energies clearly indicate the presence of a satellite at the binding energy position of 7.2 eV. In the cases of both as-deposited and annealed ML samples, the position and presence of this satellite peak are confirmed by varying the photon energy. The VB spectra recorded at different photon energies are shown in figure 10 and indicate enhancement in the satellite peak intensity at 67 eV which is due to the well known photoresonance effect [67]. The variation in photon energy above and below (not shown in figure 10) shows the reduction in the satellite peak intensity.

3.5.1. Variation in the Ni 3d satellite intensity and FWHM upon annealing. From measured and fitted VB spectra we have calculated the intensities of the Ni 3d VB and its satellite for both as-deposited and ML samples annealed at 400 °C and sputtered for 45 min. Similar calculations were also carried out for the Ni $2p^{3/2}$ core level and the corresponding satellite peak. Figures 11(a) and (b) show background subtracted and fitted Ni 3d VB and Ni $2p^{3/2}$ core level spectra, for both as-deposited and ML samples annealed at 400 °C. The calculated intensity of the Ni 3d satellite shows a reduction in the value of the intensity from 34% (as-deposited) to 24% (when the ML sample is annealed at 400 °C). From a similar calculation for the Ni $2p^{3/2}$ core level peak, the satellite peak intensity is found to decrease from 39% to 24%. This suggests filling of the Ni 3d band due to the formation of TiNi alloy phase at the interface upon annealing. The decrease of the Ni d^8 satellite peak intensity when Ni is alloyed with different elements is also reported by Fuggle *et al* [68] and attributed to Ni 3d band filling. In addition to this, they also report a decrease in the Ni 3d bandwidth when Ni

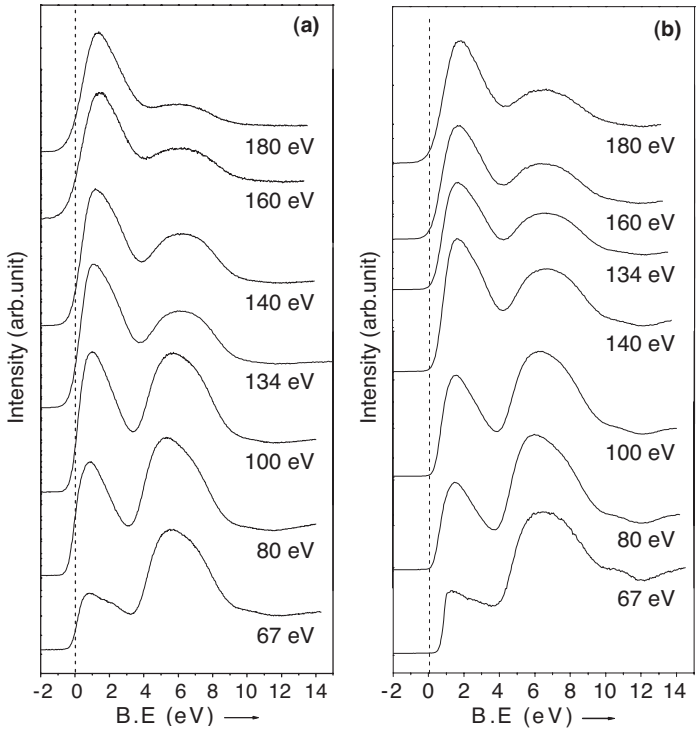

Figure 10. VB spectra recorded at different photon energies; (a) as-deposited and (b) 400 °C annealed ML samples.

Table 5. Ni 3d peak position, centroid, width, FWHM and satellite positions for as-deposited and annealed ML samples at different temperatures (all positions are in eV).

Samples	Peak position Ni 3d	Centroid	Width	FWHM	Satellite
As-deposited	0.8	1.35	4.5	2.4	6.1
200 °C	1.2	1.30	4.2	2.3	6.3
300 °C	1.5	1.73	3.8	2.4	6.7
400 °C	1.7	1.77	2.8	2.2	7.2

is alloyed with different metals. In all cases studied by them, the observed Ni d bandwidth decreases with decreasing Ni concentration. A similar type of behaviour—bandwidth decrease with decreasing Ni concentration—is also observed in the present case when the ML samples are annealed at different temperatures to form TiNi alloy phase at the interface. In the as-deposited case the bandwidth calculated using the procedure outlined in [68] is 4.5 eV and it decreases to 2.8 eV when the ML sample is annealed at 400 °C. Ni 3d band parameters such as the peak and centroid positions, widths of the Ni 3d band, FWHM and satellite positions for ML samples annealed at different temperatures are shown in table 5.

The experimentally measured VB spectra of pure Ti, Ni and TiNi alloy phase in the present study are compared with theoretically calculated density of states. The details of the computational programme and results obtained are discussed below.

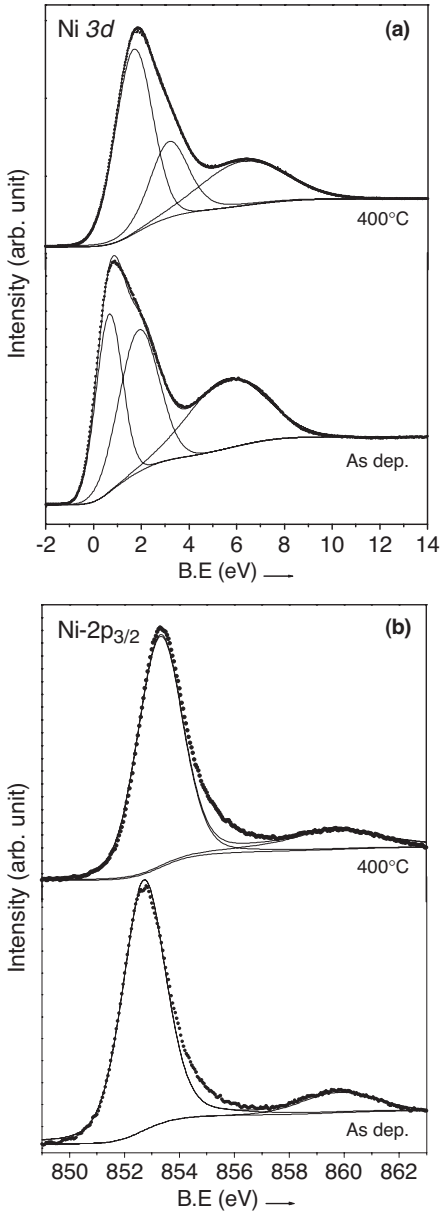

Figure 11. Fitted and background eliminated spectra of (a) the Ni 3d VB and (b) the Ni 2p core level.

3.5.2. Computational details for the FPLMTO calculations. To calculate the DOS, we have used a full potential plane wave linear muffin-tin orbital technique [69, 70] using the LMTART 6.05 code. The calculated DOS along with the experimentally observed DOS for elemental Ti, Ni and TiNi alloy phase are shown in figure 12. In general, the calculated DOS are in good agreement with experimentally recorded VB spectra except for a slight shift in the binding energy positions of Ti and Ni. In measured VB spectra, the Ni and Ti d band are observed to be shifted further to the higher binding energy side than the calculated values by 0.7 and 0.3 eV

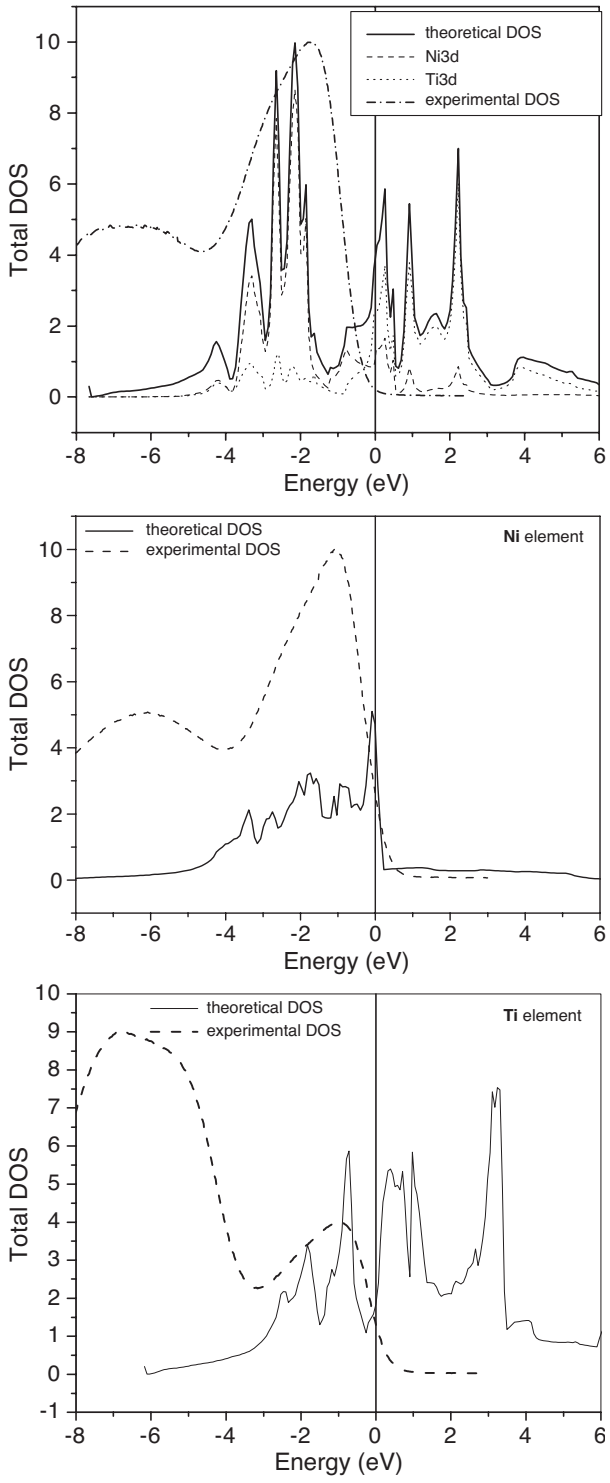

Figure 12. Theoretical and experimentally calculated densities of states; (a) Ti, (b) Ni and (c) TiNi alloy phases.

respectively. The experimentally recorded VB spectra of 400 °C annealed ML samples also show shifts in the Ni 3d bands to the higher binding energy side, by 1.1 eV. The theoretically calculated DOS of Ti, Ni and TiNi in the present case match well with the DOS for B2 TiNi phase calculated by others [71–73]. In addition to this, it can be seen that there is a reduction in the DOS of Ni 3d at the Fermi level and it is also moved to the higher binding energy side as compared to that for elemental Ni. One can also see that the Ti 3d contribution is substantially less than that of Ni 3d when they formed the TiNi alloy phase, indicating a greater possibility of Ni d band filling and localization of the Ni 3d band. The calculated percentage contribution of Ni 3d in TiNi is about 78%, whereas for Ti 3d states it is only 22%. These results suggest that in the case of TiNi alloy phase formation, the mixing of levels (3d, 4s, 4p) is mainly responsible for the band filling rather than the charge transfer process.

Thus, on the basis of the above studies we can say that the main difference in VB features observed between as-deposited and annealed Ti/Ni ML samples are therefore:

(i) the increase in the energy of the main maximum of the VB relative to the Fermi level and accordingly a shift in the centroid of the binding energy by 0.52 eV, indicating shifting of the Ni 3d band to the bottom of the VB as compared to its elemental state;
(ii) the reduction in intensity of the Ni 3d density of states at the Fermi level, indicating enhancements of the Ni 3d electron localization in the TiNi alloy phase;
(iii) the decrease in the Ni 3d satellite peak intensity due to the filling of the Ni d bands and the shift in binding energy position from 6.1 to 7.2 eV as Ni is alloyed with Ti forming the TiNi alloy phase at higher temperatures of annealing;
(iv) the decrease in the Ni 3d bandwidth due to the hybridization (mixing) between the levels of Ni and those of neighbour atoms, giving rise to the Ni–Ti–Ni type of interaction, when alloying occurs.

All these observed changes are indicative of TiNi phase at the interface in annealed ML samples.

4. Conclusion

The core level and VB photoemission measurements, along with quantitative analysis of these recorded spectra, corresponding to as-deposited as well as annealed Ti/Ni ML samples, show interesting changes in the electronic properties related to the structural modifications that have occurred in the ML stack due to annealing treatment. The depth profile core level and VB photoemission measurements made on the as-deposited sample show slight intermixing of constituent elements during deposition at the interface without any chemical phase formation. The Ti XPS Auger measurements carried out on the ML sample annealed at 200 °C and sputtered for 15 min time intervals indicate a change in the chemical environment of Ti and this is attributed to diffusion of Ni into Ti layers. The corresponding core level measurements do not show a Ni $2p^{3/2}$ peak; however, for the ML sample annealed at 300 and 400 °C the appearance of the Ni $2p^{3/2}$ peak at the binding energy position of 852.5 eV corresponding to pure elemental Ni is clear, indicating faster diffusion of Ni into Ti layers at higher temperatures of annealing. In the case of the ML samples annealed at 300 and 400 °C and sputtered for 30 min, the shift in binding energy positions of Ni $2p^{3/2}$ and Ti $2p^{3/2}$ indicates TiNi alloy phase formation at the interface. XRD measurements carried out on these ML samples show SSR leading to amorphization at 300 °C and subsequent recrystallization into the TiNi alloy phase at 400 °C.

The observed shifts in core level binding energies of Ti and Ni are found to be positive for both elements and hence electronegativity criteria cannot be used to decide on the direction

of the charge transfer in the TiNi alloy phase formed at the interface due to the annealing treatment. However, calculated modified Auger parameters show a positive value for Ti and a negative one for Ni indicating the direction of charge transfer from Ni to Ti. Similar trends have also been observed from calculated chemical shifts and charges on ionized atoms using a simple electrostatic potential model.

The evolution and modifications in the VB photoemission spectra that occurred in the ML samples due to the annealing treatment have been studied using both Mg Kα and synchrotron radiation. VB photoemission measurements carried out at the photon energy of 1256.6 eV (Mg Kα) are mainly dominated by photoemission due to Ni 3d states, while the spectra recorded using synchrotron radiation at 134 eV show the presence of an emission band mostly due to Ti 3d states. These measurements taken together indicate the intermixing of Ti and Ni layers during deposition at the interface without any chemical bonding between them in the as-deposited ML samples. The recorded VB spectra corresponding to 300 and 400 °C annealed samples and sputtering for 45 min time intervals clearly show a shift in position of Ni 3d to 1.5 and 1.7 eV from its normal position of 0.8 eV. This observed shift also supports the conclusion drawn from core level studies as regards the formation of TiNi alloy phase at the interface. In addition to this, the Ni 3d satellite structure also shows a reduction in its intensity and a shift in peak position as compared to the as-deposited case, again indicating the formation of TiNi alloy phase at the interface.

Acknowledgments

The authors would like to thank Mr S K Pandey for his help with the band structure calculation presented in this paper. We are also grateful to Mr Avinash Wadikar and Mr Satish Potdar for their help during the PES measurements and the synthesis of the Ti/Ni ML samples respectively.

References

[1] Grimmer H, Zaharko O, Mertines H-Ch and Schafers F 2001 *Nucl. Instrum. Methods Phys. Res.* A **467/468** 354
[2] Grimmer H, Böni P, Breirmeier U, Clemens D, Horisberger M, Mertins H C and Schäfers F 1998 *Thin Solid Films* **319** 73
[3] Senthil M, Boni P and Clemens D 1998 *J. Appl. Phys.* **84** 6940
[4] Wang F E, Buchler W Y and Pickart S Y 1965 *J. Appl. Phys.* **36** 3232
[5] Duerig T, Pelton A and Stockel D 1999 *Mater. Sci. Eng.* A **273–275** 149
[6] Van Humbeeck J, Stalmans R and Besselink P A 1998 *Metals as Biomaterials* ed J A Helsen and H J Breme (Chichester: Wiley) pp 73–100
[7] Shabalovskaya S A and Anderegg J W 1995 *J. Vac. Sci. Technol.* A **13** 2624
[8] Shabalovskaya S A 1995 *J. Physique Coll.* IV **5** C8 1199
[9] Clemens B M 1986 *Phys. Rev.* B **33** 7615
[10] Clemens B M 1987 *J. Appl. Phys.* **61** 4525
[11] Hollanders M A, Thijsse B J and Mittemeijer E J 1990 *Phys. Rev.* B **42** 5481
[12] Chaudhari J, Alyan S M and Jankowski A F 1994 *Thin Solid Films* **239** 79
[13] Bouhki M, Bruson A and Guilmin P 1992 *Solid State Commun.* **83** 5
[14] Somsen C, Zähres H, Kästner J, Wassermann E F, Kakeshita T and Saburi T 1999 *Mater. Sci. Eng.* A **273–275** 310
[15] Lehnert T, Tixier S, Böni P and Gotthardt R 1999 *Mater. Sci. Eng.* A **273–275** 713
[16] Bhatt P, Sharma A and Chaudhari S M 2005 *J. Appl. Phys.* **97** 043509
[17] Sella C, Mâaza M, Kâabouchi M, Monkade S E, Miloche M and Lassri H 1993 *J. Magn. Magn. Mater.* **121** 201
[18] Sella C, Mâaza M, Miloche M, Kâabouchi M and Krishnan R 1993 *Int. Coat. Tech.* **60** 379
[19] Sdaq A, Broto J M, Rakoto H, Ousset J C, Raquet B, Vidal B, Jiang Z, Bobo J F, Piecuch M and Baylac B 1993 *J. Magn. Magn. Mater.* **121** 409
[20] Porte M, Lassri H, Krishanan R, Kaabouchi M and Sella C 1993 *Appl. Surf. Sci.* **65/66** 131
[21] Kudryavtsev Y V, Nemoshkalenko V V, Lee Y P, Kim K W, Kim C G and Szymanski B 2000 *J. Appl. Phys.* **88** 2430

[22] Mahesh V, Basu S, Shubha G and Kulkarni S K 1998 *Thin Solid Films* **335** 13
[23] Chaudhari S M, Suresh N, Phase D M, Gupta A and Dasannacharya B A 1999 *J. Vac. Sci. Technol.* A **17** 242
[24] Angal-Kalinin D *et al* 2002 *Curr. Sci.* **82** 283
[25] http://www.srim.org/index.htm#HOMETOP
[26] Chaudhari S M, Phase D M, Wadikar A D, Dasannacharya B A, Ramesh G S and Hegde H S 2002 *Curr. Sci.* **82** 305
[27] Briggs D and Seah M P 1984 *Practical Surface Analysis* (New York: Wiley)
[28] Wagner C D, Riggs W M, Moulder L E and Muilenberg G E (ed) 1978 *Handbook of X-ray Photoelectron Spectroscopy* (New York: Perkin-Elmer)
[29] http://sun.phy.cuhk.edu.hk/~surface/XPSPEAK/XPSPEAKusersguide.doc
[30] Wallart X, Zeng H S, Nya J P, Dalmai G and Friedal P 1991 *J. Appl. Phys.* **69** 8171
[31] Hillerbrecht F U, Fuggle J C, Bennett P A, Zolnierek Z and Freiburg Ch 1983 *Phys. Rev.* B **27** 2179
[32] Shabalovskaya S, Narmonev A, Ivanova O and Dementjev A 1993 *Phys. Rev.* B **48** 13296
[33] Shirley D A 1972 *Phys. Rev.* B **5** 4709
[34] Burrell M C and Armstrong N R 1983 *Appl. Surf. Sci.* **17** 53
[35] Bishop H E 1981 *Surf. Interface Anal.* **3** 343
[36] Tougaard S 1990 *J. Electron Spectrosc. Relat. Phenom.* **52** 243
[37] Tougaard S 1989 *Surf. Sci.* **216** 343
[38] Seah M P 1990 *Practical Surface Analysis* vol 1, ed D Briggs and M P Seah (New York: Wiley) chapter 5
[39] Tougaard S and Sigmund P 1982 *Phys. Rev.* B **25** 4452
[40] Tougaard S 1988 *Surf. Interface Anal.* **11** 453
[41] Seabolt M A, Ogden W R, Chourasia A R and Ishida A 2004 *J. Electron Spectrosc. Relat. Phenom.* **135** 135
[42] Pauling L 1960 *The Nature of Chemical Bond* (New York: Cornell University Press) p 93
[43] Morietti G 1998 *J. Electron Spectrosc. Relat. Phenom.* **95** 95
[44] Wagner C D 1975 *Faraday Discuss Chem. Soc.* **60** 291
[45] Kowalczyk S P, Ley L, McFeely F R, Polla R A and Shirley D A 1974 *Phys. Rev.* B **9** 381
[46] Thomas T D 1980 *J. Electron Spectrosc. Relat. Phenom.* **20** 117
[47] Synder L C 1971 *J. Chem. Phys.* **55** 95
[48] Siegbahn K, Nordling C, Fahlman A, Nordberg R, Hamerin K, Hedman J and Lindberg B 1967 *Electron Spectroscopy For Chemical Analysis—Atomic, Molecular and Solid-State Structure Studies by Means of Electron Spectroscopy (Almqvist and Wilksells, Stockhom, 1967)* (*Nova Acta Regiae Soc. Sci. Ups. Ser. IV*) p 20
[49] Choi E, Oh S-J and Choi M 1991 *Phys. Rev.* B **43** 6360
[50] Johansson B and Martensson N 1980 *Phys. Rev.* B **21** 4427
[51] Willams A R and Lang N D 1978 *Phys. Rev. Lett.* **40** 954
[52] Castellani N J and Leroy D B 1988 *Z. Phys.* B **71** 315
[53] Watson R E, Hudis J and Perlman M L 1971 *Phys. Rev.* B **4** 4139
[54] Friedman R M, Hudis J, Perlman M L and Watson R E 1973 *Phys. Rev.* B **8** 2433
[55] Chou T S, Perlman M L and Watson R E 1976 *Phys. Rev.* B **14** 3248
[56] Sham T K, Perlman M L and Watson R E 1979 *Phys. Rev.* B **19** 539
[57] Wertheim G K, Cohen R L, Grecelius G, West K W and Wernick J H 1979 *Phys. Rev.* B **20** 860
[58] Olovsson W, Abrikosov I A, Johansson B, Newton A, Cole R J and Weightman P 2004 *Phys. Rev. Lett.* **92** 226406
[59] Abrikosov I A, Olovsson W and Johansson B 2001 *Phys. Rev. Lett.* **87** 176403
[60] Thomas T D and Weightman P 1986 *Phys. Rev.* B **33** 5406
[61] Sakurai K, Private communication, National Institute For Material Science, Tsukuba, Japan
[62] Ridley N and Pops H 1970 *Metall. Trans.* **1** 2867
[63] Powder diffraction file JCPDS card No 35 682 (for Ti), 34 850 (for Ni) and 339113, 314483 (for TiNi).
[64] Lehnert T, Tixier S, Böni P and Gotthardt R 1999 *Mater. Sci. Eng.* A **273–275** 713
[65] Shevchik N J 1974 *Phys. Rev. Lett.* **33** 1336
[66] Scofield J D 1976 *J. Electron Spectrosc. Relat. Phenom.* **8** 129
[67] Stefen H 1935 *Photoelectron Spectroscopy—Principle and Application* 2nd edn (Berlin: Springer) p 201
[68] Fuggle J C, Hillerbrecht F U, Zolnierek Z, Bennett P A and Freiburg Ch 1982 *Phys. Rev.* B **27** 2145
[69] Will J M and Cooper B R 1987 *Phys. Rev.* B **36** 3809
[70] Will J M and Cooper B R 1989 *Phys. Rev.* B **39** 4945
[71] Pasturel A, Colinet C, Nguyen D, Paxton A T and Van Schilfgaarde M 1995 *Phys. Rev.* B **52** 15176
[72] Cai J, Wang D S, Liu S J, Duan S D and Ma B K 1999 *Phys. Rev.* B **60** 15691
[73] Fukuda T, Kakeshita T, Houjoh H, Shiraishi S and Saburi T 1999 *Mater. Sci. Eng.* A **273–275** 166